Mapping human temporal and parietal neuronal population activity and functional coupling during mathematical cognition

Amy L. Daitch[a,1], Brett L. Foster[a,b], Jessica Schrouff[a,c], Vinitha Rangarajan[a,d], Itır Kaşikçi[a,e], Sandra Gattas[a,f], and Josef Parvizi[a,1]

[a]Laboratory of Behavioral and Cognitive Neuroscience, Stanford Human Intracranial Cognitive Electrophysiology Program, Department of Neurology and Neurological Sciences, Stanford University, Stanford, CA 94305; [b]Department of Neurosurgery, Baylor College of Medicine, Houston, TX 77030; [c]Department of Computer Science, University College London, London WC1E 6BT, United Kingdom; [d]Department of Psychology, University of California, Berkeley, CA 94720; [e]Graduate School of Neuroscience, Istanbul University, Istanbul 34393, Turkey; and [f]Medical Scientist Training Program, University of California, Irvine, CA 92697

Edited by Marcus E. Raichle, Washington University in St. Louis, St. Louis, MO, and approved October 7, 2016 (received for review May 25, 2016)

Brain areas within the lateral parietal cortex (LPC) and ventral temporal cortex (VTC) have been shown to code for abstract quantity representations and for symbolic numerical representations, respectively. To explore the fast dynamics of activity within each region and the interaction between them, we used electrocorticography recordings from 16 neurosurgical subjects implanted with grids of electrodes over these two regions and tracked the activity within and between the regions as subjects performed three different numerical tasks. Although our results reconfirm the presence of math-selective hubs within the VTC and LPC, we report here a remarkable heterogeneity of neural responses within each region at both millimeter and millisecond scales. Moreover, we show that the heterogeneity of response profiles within each hub mirrors the distinct patterns of functional coupling between them. Our results support the existence of multiple bidirectional functional loops operating between discrete populations of neurons within the VTC and LPC during the visual processing of numerals and the performance of arithmetic functions. These findings reveal information about the dynamics of numerical processing in the brain and also provide insight into the fine-grained functional architecture and connectivity within the human brain.

numerical processing | ECoG | brain network | parietal cortex | ventral temporal cortex

Although the ability to approximate or compare rough quantities is present even in human infants (1) and in other species such as nonhuman primates (2–4) and birds (5), the association of exact quantities with symbols (e.g., the numeral "10") or verbal representations (e.g., the word "ten") is unique to humans exposed to such culturally learned entities (6–8). Moreover, dissociable number- and quantity-related behavioral deficits (i.e., deficits relating to symbolic or verbal numerical representations versus abstract quantity representations) are associated with different lesion locations within the brain (9–14). These observations in part motivated the Triple Code model positing that the human brain contains three different numerical representations: symbolic, verbal, and abstract quantity, each coded in a different brain region (15, 16). The model also predicts that, depending on task demands (e.g., simple visual recognition of a numeral versus determining the larger of two numerals versus verbal naming of a numeral), all or a subset of these brain regions interact with each other (15, 16).

Neuroimaging, electrophysiology, and lesion studies in both humans and nonhuman primates have long implicated the parietal lobe, particularly the anterior segment of the intraparietal sulcus (aIPS), in abstract quantity representations irrespective of the modality of presentation (e.g., "4" vs. "four" vs. "::"), with specific neurons or neuronal populations exhibiting tuning around a preferred numerosity (4, 17–25). Moreover, brain activity within this region and its functional and anatomical connectivity with other brain regions are correlated with mathematical performance in individual subjects (26–29), and perturbation of activity in this region appears to affect mathematical performance (30–32).

Although the Triple Code model predicted the existence of a specific region within the ventral visual stream selective for symbolic numerical representations (i.e., numerals), earlier human electrophysiological recordings using event-related potentials reported relatively widespread activations in the ventral temporal cortex (VTC) during number processing (33), and earlier functional imaging studies were unable to localize a region selective for numerals relative both to other culturally learned symbols (e.g., letters) and novel morphologically similar stimuli (i.e., false fonts) (17, 34–36). Recently, our group used intracranial electrocorticography (ECoG) to confirm the existence of a site within the posterior inferior temporal gyrus (pITG) that selectively responds to visual numerals relative to letters, false fonts, number words, and words (37). This pITG site is located in an area subject to strong susceptibility artifact with fMRI (38, 39); however, numeral selectivity within the pITG has since been demonstrated with fMRI using advanced techniques to increase the signal-to-noise ratio in this region (38, 39). Still, given the relatively low temporal resolution of the current imaging methods, it is difficult to study the

Significance

Humans have the unique ability to perform exact mental arithmetic, which derives from the association of symbols (e.g., "3") with discrete quantities. Using direct intracranial recordings, we measured electrophysiological activity from neuronal populations in the lateral parietal cortex (LPC) and ventral temporal cortex (VTC) that are known to be important for numerical processing as subjects performed various experiments. We observed functional heterogeneity within each region at the millimeter and millisecond scales and report empirical evidence of functional coupling between the LPC and VTC during mathematical cognition. Our results suggest the presence of an anatomically selective numerical cognition system that engages discrete neuronal populations of the ventral temporal and lateral parietal regions in different time windows of numerical processing.

Author contributions: A.L.D., B.L.F., and J.P. designed research; A.L.D., B.L.F., V.R., I.K., and S.G. performed research; J.S. contributed new reagents/analytic tools; A.L.D. and I.K. analyzed data; and A.L.D. and J.P. wrote the paper.

The authors declare no conflict of interest.

This article is a PNAS Direct Submission.

[1]To whom correspondence may be addressed. Email: jparvizi@stanford.edu or adaitch@stanford.edu.

This article contains supporting information online at www.pnas.org/lookup/suppl/doi:10.1073/pnas.1608434113/-/DCSupplemental.

fast temporal dynamics of activity within and surrounding the pITG and its interaction with other regions involved in numerical cognition such as the intraparietal sulcus (IPS).

In the current study, we took advantage of simultaneous ECoG recordings from discrete neuronal populations within the human VTC and lateral parietal cortex (LPC) to study the fast temporal dynamics of their activations and functional coupling during numerical conditions. We expand upon previous work and demonstrate that the brain regions within the VTC and LPC thought to represent the symbolic and abstract quantity numerical codes, respectively, are in fact each composed of heterogeneous neuronal populations with distinct temporal profiles of activity. The distinct profiles of activity in subpopulations of the VTC or LPC are mirrored by their distinct patterns of functional coupling. Our results suggest the existence of multiple feedback loops between different subpopulations of the VTC and LPC that operate during different stages of numerical processing. These findings provide insight into the mechanics of numerical processing in the brain and also have implications for studying the fine-grained architecture of the brain's functional connections in general.

Results

Sixteen patients with epilepsy were implanted with intracranial electrodes as part of their presurgical evaluation at Stanford University Medical Center and volunteered to participate in our research study. Demographic information for these subjects and their behavioral performance are included in Table S1, and each subject's electrode coverage is displayed in Fig. S1. We obtained ECoG data during three different experimental tasks (Fig. 1). Task 1 presented subjects with single numerals, letters, or foreign symbols (i.e., false fonts), allowing us to identify numeral-selective neuronal populations. Task 2 required subjects to manipulate numerals actively by assessing the validity of arithmetic statements (versus the control condition of assessing the validity of memory statements). In task 3, subjects were required to assess the validity of arithmetic statements (as in task 2), but each arithmetic equation was presented one symbol at a time (e.g., "7," "+," "5," "=," "12"), allowing us to track better the temporal profile of activity of each region during different stages of arithmetic processing. On average, subjects performed with greater than 85% accuracy on each task; the variation between subjects' accuracy and reaction time in all tasks is presented in Table S1.

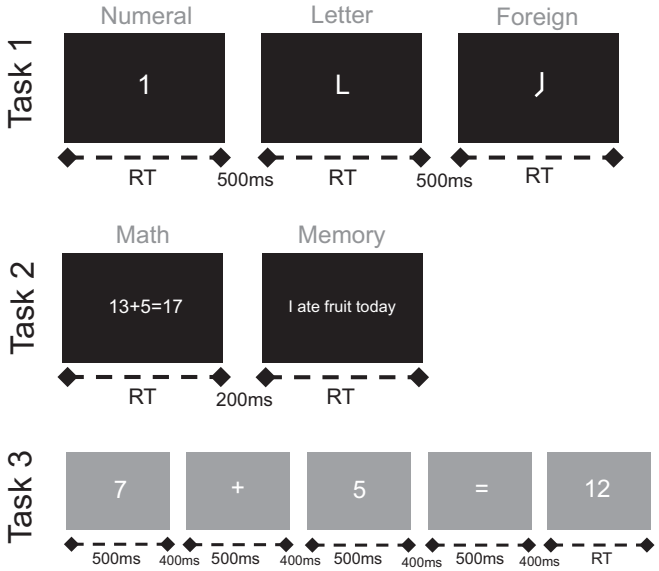

Fig. 1. Illustration of the three behavioral tasks. See *Experimental Procedures* for a detailed description of each task.

Our analyses were aimed first at characterizing the response properties of subregions within the VTC and LPC to confirm the presence of numeral- and/or math-selective neuronal populations that we and other groups have reported previously (20, 22, 23, 37, 39, 40). Next, we measured the relative timing of the activation of each of these regions during arithmetic computations. Finally we assessed the functional coupling between the VTC and LPC during arithmetic computations.

Selectivity of the Response to Numerals Within the VTC. We measured the activity and selectivity of each electrode across a wide range of frequencies (1–256 Hz) but found that high-frequency broadband (HFB; 70–180 Hz) activity best differentiated between numeric and nonnumeric conditions (Fig. S2). Further, in line with recent work from our group (41), we found that support vector machine (SVM) classifiers on the data from task 2 differentiated between math and memory trials most accurately, both on average and in each individual subject (Fig. S2*E*), when using HFB activity rather than activity in five other frequency bands. The HFB classifiers also were the only ones with classification accuracy significantly above chance in every subject [permutation test, $P < 0.05$, false-discovery rate (FDR) corrected]. These findings corroborate previous work showing a high correspondence between HFB activity and local neuronal firing rate and with fMRI blood-oxygen level-dependent activity (42–47). Because selectivity for the different stimulus classes/trial types was most prominent in the HFB band, we focused on HFB activity in subsequent analyses.

Although many sites within the VTC responded significantly to the presentation of numerals (relative to the intertrial interval, ITI), a small subregion within the pITG responded selectively to numerals compared with morphologically similar stimuli such as letters and false fonts [3 of 58 of all pITG sites (5.2%), $P < 0.05$, FDR-corrected, in 3 of the 13 subjects with pITG coverage; or 7 of 58 electrodes (12%), $P < 0.05$, FDR uncorrected, from four different subjects, all with right hemisphere coverage] (Fig. 2 *C* and *D*, Fig. S3, and Table S2). We refer to this numeral-selective pITG site as the "number form area" (NFA). These findings in a new subcohort of subjects confirmed our previous report of a numeral-selective brain region (37).

Also in line with a recent report from our group (40), we found sites bilaterally within a broader region of the pITG that were selectively engaged during arithmetic processing, relative to reading sentences/memory retrieval (task 2), although by and large their response to single numerals were insignificant and/or not significantly different from their responses to single letters or false fonts (31 of 58 sites, 53%; $P < 0.05$, FDR-corrected) (Fig. 2*C*, Fig. S3, and Table S2). We refer to this pITG region as "$pITG_{math}$." This region includes the NFA itself, which also was selectively engaged during math in task 2. Although we recorded from the NFA proper in only three subjects after FDR correction (in four subjects before FDR correction), we observed at least one math-selective pITG site in all 13 subjects implanted with pITG electrodes (Table S2).

As in task 1, many sites throughout the VTC were significantly active during arithmetic processing, and many sites outside the pITG, particularly in the posterior VTC, responded more strongly during arithmetic processing than did sites within the pITG (Fig. 2*B*). However, the region that was most selectively engaged during arithmetic processing (and was not engaged during reading/memory retrieval) was anatomically similar to, although larger in size than, the NFA (Fig. 2, Fig. S3, and Table S2).

It is important to note that even within the $pITG_{math}$ area there exists much heterogeneity in the profile of responses to different types of numerical stimuli, even within a few millimeters of cortex. Fig. S4 shows an example of such heterogeneity in

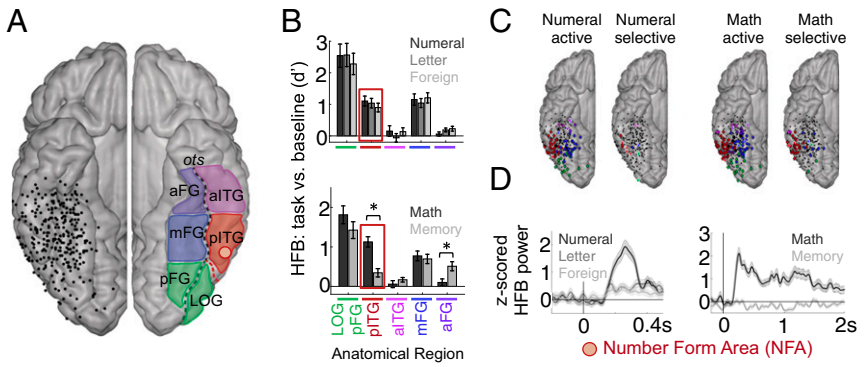

Fig. 2. (*A*) Electrodes within the VTC. The placement of electrodes in all 14 subjects who had electrodes over the VTC is projected onto the right hemisphere of an atlas brain. The anatomical subdivisions within the VTC considered in this study are shown on the left hemisphere. aFG, anterior fusiform gyrus; aITG, anterior inferior temporal gyrus; LOG, lateral occipital gyrus; mFG, midfusiform gyrus; pFG, posterior fusiform gyrus; pITG, posterior inferior temporal gyrus. (*B*) HFB responses to numerals and other visual symbols in task 1 (*Upper*) and when analyzing math or memory statements in task 2 (*Lower*), grouped by sites in each VTC subregion, averaged across all subjects. Error bars indicate SE across electrodes. Asterisks indicate a significant difference in HFB response between math and memory conditions (after FDR correction). Note that the selectivity of individual electrodes within a region of interest (ROI) may be different from the average selectivity of that ROI. (*C*) Highlighted are individual electrodes across all subjects that are significantly numeral active relative to the ITI (brain at far left), numeral selective relative to letters and foreign symbols (second brain from left), math active relative to the ITI (third brain from left), and math selective relative to memory and also with no significant memory response (brain at right). The color of each electrode denotes its anatomical region (determined in individual brain space). Electrodes outlined in black have significant responses at the level of $P < 0.05$, FDR-corrected, and those outlined in white are significant at $P < 0.05$, uncorrected. (*D*) Exemplar HFB time courses during task 1 and task 2 are shown for an exemplar NFA site (from subject S13). The shaded area represents the SE across trials for each condition.

a single subject across tasks 1–3. One site is within the NFA, responding selectively to numerals relative to other symbols in tasks 1 and 3 and with a sustained math-selective response in task 2. Further, in task 3 this site responds more to the second numeral than the first numeral, likely reflecting an increased engagement of this site during computations. The two neighboring sites are each only 5 mm away from the NFA site, but they exhibit different response properties, responding less selectively to numerals in tasks 1 and 3 and with more transient math-selective responses in task 2. Thus, although we group the $pITG_{math}$ sites together, we acknowledge that this region is in fact composed of several neuronal populations with slightly different functional profiles of activity and likely with different patterns of interaction with other brain regions (e.g., the IPS). Given the relative sparsity of electrode sampling with respect to the size of these neuronal populations, it is not surprising that we recorded from NFA proper in only a few subjects (Fig. S3 and Table S2). In subsequent analyses, based on task 2, we focused on $pITG_{math}$ sites that included the NFA sites.

Also of note, the number/math-selective region described above is anatomically distinct from other category-selective regions within the VTC, such as the fusiform face area (FFA) (46) and the word form area (WFA), sites that responded selectively to letters in task 1 and/or to written memory statements in task 2 (Fig. S3). It is particularly noteworthy that the NFA and WFA are anatomically distinct, because numbers and letters are morphologically similar symbols, composed of lines and curved segments. Thus it is unlikely that the NFA/$pITG_{math}$ region codes for purely visual aspects of numerical stimuli.

Numerical Processing Within the Parietal Cortex. We partitioned the parietal cortex into six anatomical divisions based on each individual's native anatomy (Fig. 3*A*) and measured in each region the average HFB response to the presentation of visual numerals (task 1) and active mathematical computations (task 2).

Although several sites, mostly within the superior parietal lobule (SPL) were significantly active during the presentation of numerals (relative to the ITI), no LPC sites responded selectively to single visual numeral symbols relative to letters or false fonts (Fig. S3 and Table S2). By comparison, in task 2, when subjects

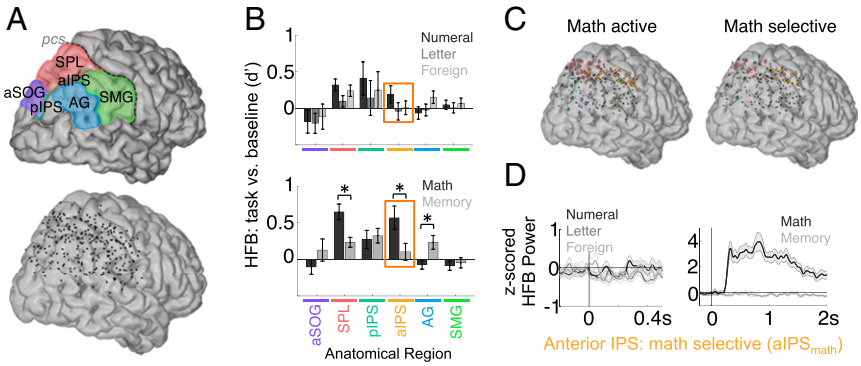

Fig. 3. (*A*) Electrodes within the LPC. The placement of electrodes in all 14 subjects with electrodes over the LPC is shown on the right hemisphere of an atlas brain (*Lower*). Also shown are the anatomical subdivisions within the LPC considered in this study (*Upper*). AG, angular gyrus; aIPS, anterior intraparietal sulcus; aSOG, anterior superior occipital gyrus; pIPS, posterior intraparietal sulcus; SMG, supramarginal gyrus; SPL, superior parietal lobule. (*B*) HFB responses to numerals and other visual symbols in task 1 (*Upper*) and when analyzing math or memory statements in task 2 (*Lower*), grouped by sites in each LPC subregion, averaged across all subjects. Error bars indicate SE across electrodes. Asterisks indicate a significant difference in HFB response between math and memory conditions (after FDR correction). (*C*) Highlighted are individual electrodes across all subjects that are significantly math active relative to the ITI (*Left*) and math selective relative to memory and also with no significant memory response (*Right*). The color of each electrode denotes its anatomical region as determined in individual brain space. Electrodes outlined in black have significant responses at the level of $P < 0.05$, FDR-corrected, and those outlined in white are significant at $P < 0.05$, uncorrected. (*D*) Exemplar HFB time courses during task 1 and task 2 are shown for a site in the aIPS of S11 that does not respond to the passive presentation of numerals, letters, or false fonts but is selectively engaged during active mathematical computation. The shaded area represents the SE across trials for each condition.

actively manipulated numerals in arithmetic computations, we found that the aIPS and SPL were more engaged during arithmetic processing than during reading sentences/memory retrieval ($P < 0.05$, FDR-corrected) (Fig. 3*B*, Fig. S3, and Table S2). We refer to these math-selective regions, which we observed in both the right and left hemispheres, across many subjects (9 of 13 subjects with SPL coverage and 8 of 13 subjects with aIPS coverage) (Table S2) as "$aIPS_{math}$" and "SPL_{math}." Conversely, in line with other recent findings (47), sites in the angular gyrus were more active during memory retrieval than during arithmetic processing ($P < 0.05$, FDR-corrected) (Fig. 3*B* and Fig. S3). Importantly, most of the math-selective sites in the aIPS and many in the SPL were not significantly active during memory trials (Fig. 3 *C* and *D*, Fig. S3, and Table S2). By comparison, we did observe many sites in more posterior portions of the IPS and in the SPL exhibiting a transient response at the beginning of both math and memory trials (e.g., see Fig. S6*E*).

Temporal Dynamics of VTC and LPC Activity During Numerical Processing. The two previous analyses mapped out the VTC and LPC subregions that are selective for either the visual presentation or arithmetic manipulation of visual numerals. Next, we addressed the temporal profile of activations within these two regions by computing the response onset latency (ROL) of HFB activity in each of these conditions (task 1 and task 2) and comparing the response of each region in different stages of arithmetic processing in task 3. For the ROL analysis, we considered only the sites that were significantly active during the presentation of numerals (task 1) and/or arithmetic processing (task 2), because we could measure ROL reliably only for sites exhibiting a clear increase in activity. The majority of these sites were located in the lateral occipital gyrus (LOG)/posterior fusiform gyrus (pFG), pITG, and midfusiform gyrus (mFG) (for both numerals and math) and in the aIPS and SPL (for math). To assess differences in ROL between brain regions, we considered only pairs of electrodes within individual subjects so that differences in overall processing speed between subjects would not alter our general findings.

In task 1, the pITG sites responded to the visual presentation of numerals later than did sites in the LOG/pFG by 35 ± 26 (SD) ms and the mFG by 46 ± 42 ms ($P < 0.05$, FDR-corrected) (Fig. 4 *A*–*C*). Similarly, in task 2, math-active sites in the pITG responded significantly later than those in the LOG/pFG by 51 ± 20 ms and mFG by 60 ± 42 ms ($P < 0.05$, FDR-corrected) (Fig. 4 *D*–*F*). Furthermore, within the pITG, neuronal populations that were active during the math but not during the memory condition responded significantly later during the math condition than those that were active during both math and memory trials by 47 ± 21 ms ($P < 0.001$, FDR-corrected). Likewise, within the SPL and aIPS, math-selective sites that were not significantly active during memory trials responded later than those that were significantly active during both math and memory trials by 170 ± 100 ms ($P < 0.02$, FDR- corrected). These findings provide further evidence that these math-selective sites within the VTC and LPC are involved in higher-level rather than purely visual processing of numerals.

We next measured activity during task 3 (performed by 9 of 16 subjects) (Table S1) to compare more explicitly the engagement of different brain regions during different stages of numerical processing. In line with our observations from task 2, we found that pITG and aIPS math-active sites exhibited a larger response to the second numeral than to the first numeral (Fig. 5). Some of

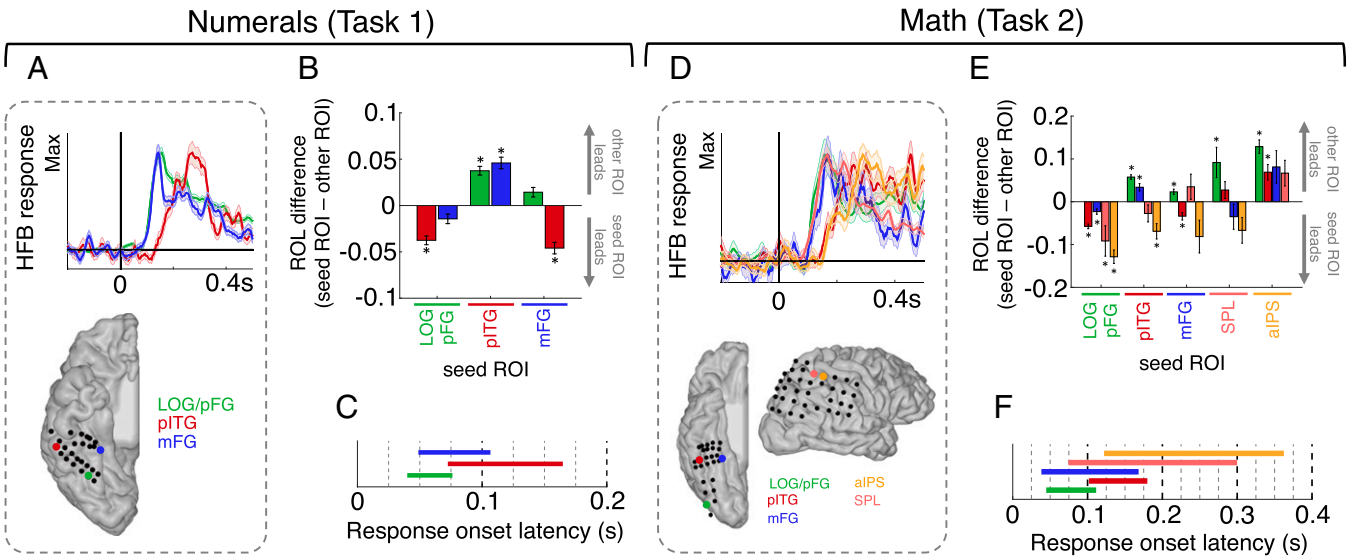

Fig. 4. (*A*) Exemplar HFB time courses during the numeral condition in task 1 at sites within three different VTC regions in a single subject (S13). The HFB time course at each site is scaled by its own maximum. The shaded area represents the SE across trials for each condition. Note that the pITG site responds later to numerals than either the pFG or mFG site. (*B*) Group-averaged differences between the HFB ROL to numerals at electrode pairs in different anatomical regions. Only electrode pairs within an individual subject were considered. Number of electrode pairs per ROI-pair: LOG/pFG-pITG: 44 pairs across four subjects; LOG/pFG-mFG: 34 pairs across four subjects; pITG-mFG: 45 pairs across seven subjects. Asterisks denote significant differences in ROL between two anatomical regions (*$P < 0.05$, FDR-corrected). (*C*) The approximate range of the ROL to numerals for each anatomical region is plotted in seconds. Data are shown as mean ± 1 SD across all subjects and all electrodes. (*D*) Exemplar HFB time courses during the math condition in task 2 at sites within three different VTC subregions and two LPC regions in a single subject (S4). The HFB time course at each site is scaled by its own maximum. The shaded area represents the SE across trials for each condition. Note that in this subject the pITG and aIPS sites respond after the LOG/pFG, mFG, and SPL sites and respond nearly simultaneously with each other. (*E*) Group-averaged differences between the HFB ROLs during the math condition (task 2) at electrode pairs in different anatomical regions. Only electrode pairs within an individual subject were considered. Number of electrode pairs per ROI-pair: LOG/pFG-pITG: 23 pairs across five subjects; LOG/pFG-mFG: two pairs across one subject; LOG/pFG-SPL: four pairs across one subject; LOG/pFG-aIPS: six pairs across two subjects; pITG-mFG: 14 pairs across five subjects; pITG-SPL: 17 pairs across four subjects; pITG-aIPS: 14 pairs across four subjects; mFG-SPL: six pairs across two subjects; mFG-aIPS: five pairs across two subjects; SPL-aIPS: 11 pairs across four subjects. Asterisks indicate significant differences in ROL between two anatomical regions (*$P < 0.05$, FDR-corrected). (*F*) The approximate range of the ROL to math for each anatomical region is plotted in seconds. Data are shown as mean ± 1 SD.

these $pITG_{math}$ and $aIPS_{math}$ sites showed almost no HFB response until after the presentation of the second numeral (Fig. 5*B*), suggesting that these regions are likely involved in the manipulation of numerals during a computation rather than merely in the visual processing of numerals. Sites in LOG/pFG, mFG, and SPL, on the other hand, responded less to the second numeral than to the first numeral (Fig. 5*C*), possibly reflecting visual adaptation to the numeral stimuli.

After comparing onset latencies of math-active sites separately within the VTC and within the LPC, we next measured the time difference between the onsets of activation occurring in the math-selective regions within the VTC and LPC. Although 12 subjects had simultaneous coverage in the VTC and LPC, only three (subjects S2, S4, and S11) had at least one site each in the aIPS and pITG with sufficiently strong math-related responses in task 2 to measure onset times reliably. Across these three subjects, the onset times of $pITG_{math}$ sites were earlier on average than those of $aIPS_{math}$ sites by 54 ± 85 ms ($P < 0.05$, FDR-corrected) (Fig. 4*E*). However, we did observe nearly simultaneous onsets of activity in the most math-selective aIPS site and the two most math-selective pITG sites in a single subject (S4); exemplar time courses are shown in Fig. 4*D*; permutation test, $P > 0.05$. One of the same three subjects, S11, also performed task 3, giving us more detailed information about the engagement of VTC and LPC activation in different stages of numerical processing. Again, we found that the most math-selective pITG and aIPS sites responded nearly simultaneously to the presentation of the second numeral (permutation test, $P > 0.05$; neither site responded much to the first numeral, as shown in Fig. 5*B*).

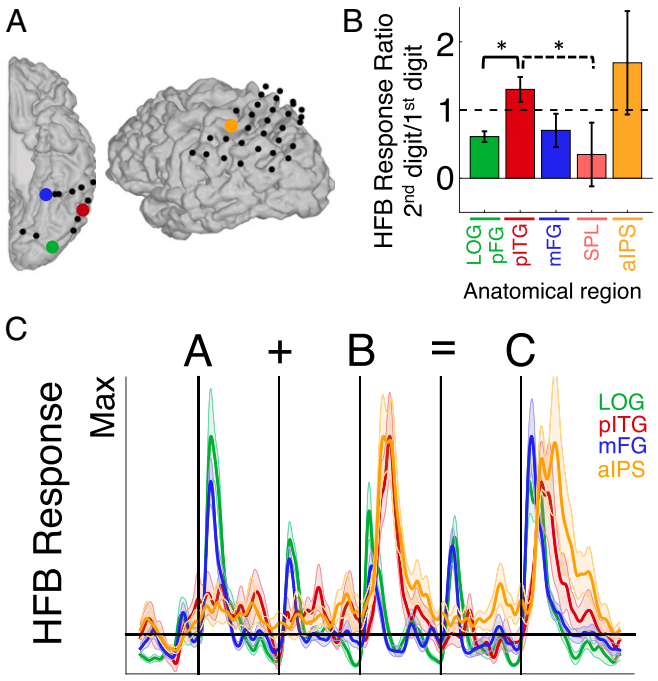

Fig. 5. (*A*) Math-active sites in four different anatomical regions in an exemplar subject (S11; this subject had no math-active SPL sites). (*B*) HFB time course during task 3 at each site in *A* (scaled by each site's own maximum). The shaded area represents the SE across trials for each condition. Note that although the pITG and aIPS sites respond more to the second digit than to the first digit, the pFG and mFG sites respond more to the first digit than to the second digit (the pITG site shown here is not within the NFA). (*C*) At the group level, the ratio of the HFB response to the second digit relative to the response to the first digit was larger than 1 in the pITG and aITG and was less than 1 in the LOG/pFG, mFG, and SPL. Brackets represent significant differences in the ratio between regions (solid bracket: $P < 0.05$, FDR-corrected; dashed bracket: $P < 0.05$, uncorrected). Error bars indicate SE across electrodes.

In addition to the nearly simultaneous engagement of subpopulations within the pITG and aIPS during numerical processing, we observed that the math-selective sites in these regions also exhibited a more sustained response during numerical processing than did other active but less selective sites. Specifically, we measured the trial-by-trial correlation between the duration of HFB responses and behavioral reaction time at each electrode site separately during math and memory trials in task 2. A high correlation between HFB duration and RT during math trials suggests that a site exhibits sustained activity throughout an arithmetic computation. Although some sites exhibited a transient response at the beginning of both math and memory trials (i.e., a response whose duration was uncorrelated with reaction time; e.g., the mFG site in Fig. S5*A*, *Top Row*), many sites within the pITG and aIPS exhibited a sustained HFB response during math trials but not during memory trials, and the duration of the response was correlated with reaction time (e.g., Fig. S5*A*, *Middle* and *Bottom*). On average, in the pITG, aIPS, and SPL, the correlation between HFB duration and RT was significantly higher during math trails than during memory trials ($P < 0.05$, FDR-corrected; pITG: average $r = 0.38$ for math vs. $r = 0.15$ for memory; aIPS: $r = 0.37$ vs. $r = 0.22$; SPL: $r = 0.38$ vs. $r = 0.26$), but the correlation was not significantly different between math and memory trials in other VTC or LPC regions (Fig. S5*B*).

Task-Dependent Correlation of Activity Between the LPC and VTC. The similar temporal profiles of activity in the pITG and aIPS in the same individual suggest a possible coupling of computations taking place in these sites. However, to assess the presence of possible functional coupling between discrete VTC and LPC populations more directly, we measured the correlation of trial-to-trial HFB power fluctuations between different regions of the LPC and VTC during both math and memory trials in task 2. For this analysis, we included only the five subjects with at least one $pITG_{math}$ and one $aIPS_{math}$ site (Table S2). Although we expected the activity between a pair of sites in the $pITG_{math}$ and $aIPS_{math}$ to be correlated across all task conditions (because both sites are active during math trials and are less active during memory trials), we were more interested in the correlation of activity within a particular trial type (i.e., beyond the average task response). These trial-by-trial fluctuations in activity beyond the average stimulus-induced response (often termed "noise correlations") are thought to reflect variations in endogenous activity from trial to trial; thus a significant correlation in noise between sites suggests a functional interaction between those sites. Such noise correlations have been shown to recapitulate patterns of activation during a task and have been linked to putative functional networks (47–52). Using intracranial recordings, our group recently showed that regions of the putative default mode network exhibit correlated HFB activity individually within different task conditions but most strongly during memory retrieval, when this network is known to be engaged (47). Here, we similarly found the HFB activity between the $pITG_{math}$ and $aIPS_{math}$ sites to be highly correlated during math trials and less so during memory trials (Fig. 6 *A–C* and Fig. S6 *A–D*). Importantly, during the math condition pITG and aIPS exhibited more correlated activity with each other than with other anatomically closer regions (i.e., with other VTC regions for the pITG and with other parietal regions for the aIPS) (Fig. S6 *B* and *D*). Also of note, the aIPS still exhibited more correlated activity with the pITG than with the LOG/pFG during memory trials (Fig. 6*C*), suggesting an intrinsic coupling between these two regions.

Importantly, many VTC sites outside the $pITG_{math}$ region exhibited larger HFB responses during math trials (although nonselectively compared with the $pITG_{math}$ sites) (Figs. 2*B* and 6*B* and Fig. S6*F*); however these regions were not as highly correlated

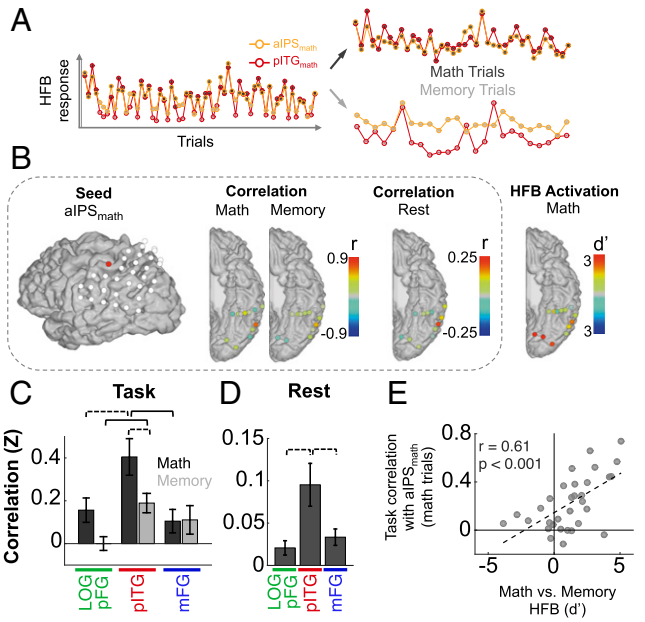

Fig. 6. (*A*) Illustration of trial-by-trial HFB correlation between an exemplar pITG$_{math}$ site and an aIPS$_{math}$ site in a single subject (S11) across all conditions (*Left*; dark filled circles are math trials, light filled circles are memory trials), only math trials (*Upper Right*), or only memory trials (*Lower Right*). (*B*) For the same subject, we show the HFB correlation between the aIPS$_{math}$ seed and each VTC site during math trials and memory trials in task 2. Also shown is the correlation of slow fluctuations of HFB power between the aIPS$_{math}$ seed and each VTC site while subjects are at rest and the level of HFB activity during math trials relative to the ITI. (*C*) Average correlation (Fisher-z) between HFB power at the aIPS$_{math}$ seed and at each VTC subregion, averaged across the five subjects (S2, S4, S8, S11, and S16) who had coverage of both aIPS$_{math}$ and pITG$_{math}$, during math trials (dark gray bars) and memory trials (light gray bars) in task 2. Significant differences in correlation between regions or task conditions are denoted with solid brackets ($P < 0.05$, FDR-corrected) and dashed brackets ($P < 0.05$, uncorrected). (*D*) Average correlation (Fisher-z) between slow fluctuations of HFB power at the aIPS$_{math}$ seed and each VTC subregion at rest, averaged across all five subjects. (*E*) Scatterplot showing the relationship between selectivity of VTC sites for math relative to memory processing and their trial-by-trial HFB correlation with aIPS during math trials. Only VTC sites that were significantly active during math trials are included.

with the aIPS$_{math}$ during math trials. In other words, the strength of HFB response alone was not predictive of a VTC site's correlation with the aIPS during math processing ($r = 0.2451$, $P = 0.1763$). Instead, the degree of selectivity of the math-active sites (relative to memory processing) within the VTC was positively correlated with the degree of their functional coupling with the aIPS during mathematical processing ($r = 0.6015$, $P = 0.0003$) (Fig. 6*E*). The same was true for LPC sites: The most math-selective sites within the LPC exhibited the most correlated activity with pITG$_{math}$ during math processing ($r = 0.3357$, $P = 0.0342$), whereas the HFB magnitude of each LPC site alone was not significantly related to its correlation with the pITG$_{math}$ ($r = 0.2831$, $P = 0.0767$) (Fig. S6 *F* and *G*). These results reinforce the notion that the observed functional coupling between pITG$_{math}$ and aIPS$_{math}$ likely reflects an interaction between them rather than mere simultaneous coactivation during numerical processing.

Intrinsic Correlation of Activity Between the LPC and VTC During Rest. Next, we explored the possibility that the pITG and aIPS are part of the same intrinsic functional network, exhibiting spontaneously correlated activity even outside the context of explicit numerical tasks. Inspired by previous work looking at the functional coupling of local field potential/ECoG activity between brain regions within putative functional networks (47, 48, 53–57), we measured the correlation of slow fluctuations (<1 Hz) of HFB activity at the VTC and LPC during rest and found higher correlations between the math-active sites within the pITG and aIPS than between these sites and other VTC or LPC sites (Fig. 6 *B* and *D* and Fig. S6 *A*–*D*). Of note, although the aIPS was more correlated with the pITG than with other nearby sites in the SPL during active math processing, the aIPS also was highly correlated with the SPL at rest (Fig. S6 *A* and *B*). This observation suggests that, although the aIPS exhibits broad local functional connectivity at rest, these local functional connections become sharpened once a subject engages in mathematical processing.

Cross-Frequency Coupling Between the IPS and VTC During Numerical Processing. Last, we aimed to understand the direction of coupling between the pITG and aIPS. Inspired by the evidence for the functional importance of low-frequency oscillations in the spatiotemporal organization of neural activity (58–60) and the coupling of the phase of low-frequency oscillations with the amplitude of higher-frequency activity (i.e., phase–amplitude coupling, PAC) (60–65), we measured the magnitude of bidirectional PAC between the aIPS and different VTC sites during both math and memory tasks.

Across the five subjects with coverage of both pITG$_{math}$ and aIPS$_{math}$ sites, the aIPS$_{math}$ low-frequency phase (in the resonant frequency band of each aIPS$_{math}$ site; see *Experimental Procedures* for more details) modulated the HFB power more on average at pITG sites than at other VTC regions (Fig. 7 *A* and C and Fig. S7). However, this pattern was not evident in the two subjects (S8 and S16) who had the weakest math responses in the aIPS (Fig. S7), perhaps because our electrodes in these subjects were located at the edge of the aIPS math-selective hub, weakening any potential observable coupling. The degree of PAC was higher, on average, from the aIPS$_{math}$ to the pITG than vice-versa, suggesting stronger top-down (aIPS$_{math}$ to pITG) than bottom-up coupling (paired permutation test, $P < 0.05$). Although interelectrode coupling was strongest between the aIPS and pITG relative to other VTC regions, there was no correlation between intraelectrode coupling at each VTC site and its interelectrode coupling with the aIPS ($r = 0.0061$, $P = 0.9651$) (Fig. 7*C*). Thus, it is unlikely that the observed aIPS–pITG coupling is simply an artifact of simultaneous coupling within the aIPS and within the pITG at the same frequencies.

Of note, the most dominant coupling frequency in the aIPS$_{math}$ sites (i.e., the frequency whose phase was most coupled to the HFB power at the same aIPS site and also to the HFB power at the pITG sites) differed across subjects (Fig. S7). In two of three subjects (S4 and S11), the coupling was most prominent within the 1–4 Hz range, whereas in the third subject (S2) the coupling was most prominent in the 7–28 Hz range. Although previous studies have shown that the dominant oscillatory frequency/coupling frequency varies across cortical areas (62, 65–68), it is somewhat surprising to see this variance even within a small patch of cortex. We are mindful that the electrode sites labeled as aIPS$_{math}$ or pITG$_{math}$ may not have recorded from the same populations of neurons across individuals, and thus the PAC findings in our small cohort of subjects should be taken as preliminary. Future work using denser and wider simultaneous sampling of the aIPS and pITG will be necessary to see if there are common coupling frequencies within specific aIPS populations across subjects.

Also of note, although on average the coupling was stronger from the aIPS to the pITG than vice versa, some pITG sites in two subjects (S2 and S4) did show stronger bottom-up coupling to the aIPS site (Fig. 7 and Fig. S7). In these subjects, the strongest coupling was from the pITG site that responded most to the passive presentation of visual numerals, and the site showing the strongest top-down PAC from the IPS was slightly

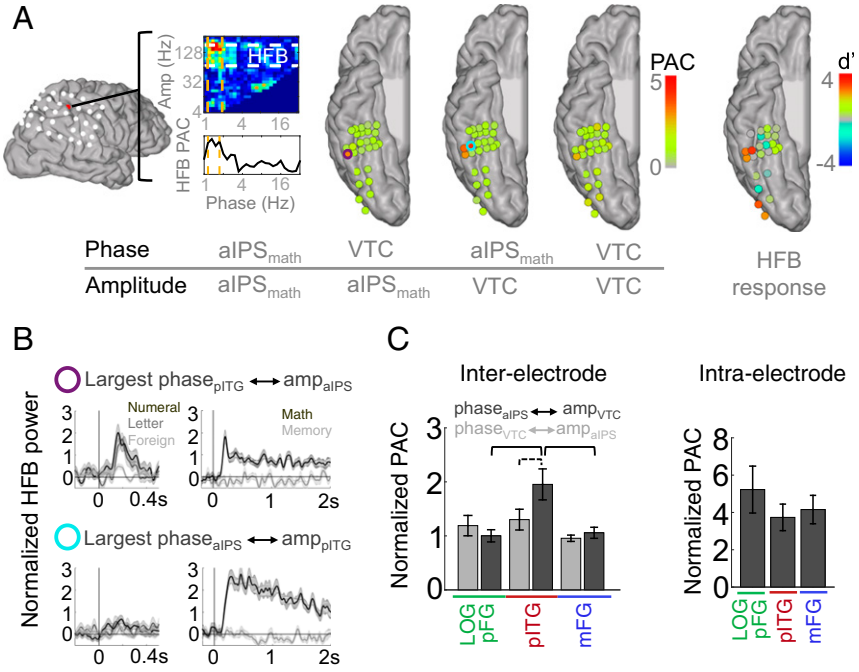

Fig. 7. (*A*) In a single subject (S4), we show PAC within the math-selective aIPS site (*Far Left*). The low-frequency band whose phase is most coupled to the HFB power at the same aIPS site is demarcated by the yellow dashed lines. The second and third images from the left show the coupling of aIPS phase to VTC HFB amplitude and of VTC phase to aIPS HFB amplitude. Note that the aIPS phase is most coupled to the HFB amplitude at sites within the pITG. The fourth image from the left shows the coupling of the phase at each VTC site to the HFB amplitude at the same site. The image on the right shows the magnitude of the HFB response at each VTC site during math trials relative to the ITI. Note that the sites with the most PAC during math trials are not necessarily the ones with the largest HFB response. (*B*) In the same subject, we show the response properties of the site showing the highest bottom-up PAC (pITG to aIPS) (*Upper*) and the site showing the highest top-down PAC (aIPS to pITG) (*Lower*). Note that the pITG site with the largest bottom-up coupling responded to the passive presentation of visual numerals (task 1) but did not show much response during active mathematical computation (task 2), whereas the site showing the strongest top-down PAC from the IPS was slightly more anterior and did not show a strong response to the passive presentation of visual numerals but showed selective activity during active mathematical computation. (*C*, *Left*) Average PAC between aIPS$_{math}$ and three different regions within the VTC averaged across the five subjects with simultaneous aIPS$_{math}$ and pITG$_{math}$ coverage. (*Right*) Average within-site PAC in each of three different regions within the VTC averaged across the same five subjects. Error bars indicate SE across electrode pairs (left) or across electrodes (right). Significant differences in PAC are denoted by solid brackets ($P < 0.05$, FDR corrected) and dashed brackets ($P < 0.05$, uncorrected).

more anterior and was engaged only during active mathematical computation and not during the passive presentation of visual numerals (data for one subject are shown in Fig. 7 *A* and *B*). Again, this finding is quite preliminary, but it is suggestive of a feedback loop between different subpopulations of the pITG and aIPS in which the pITG neuronal populations engaged in deciphering visual symbols have bottom-up coupling with the aIPS, and the aIPS has top-down coupling with more anterior neuronal populations of the pITG that are engaged in the active processing of numeral symbols.

Discussion

Recordings from the VTC and LPC in human subjects reconfirmed the existence of numeral/math-selective hubs within the VTC and LPC and also revealed functional heterogeneity within each of these regions at the millimeter scale. We report discrete neuronal populations localized within the pITG and aIPS with selective activations during conditions of numerical processing, surrounded by other active, but less selective neuronal populations. The most math-selective sites within the pITG and aIPS respond later than other active but less selective sites within the VTC and LPC, suggesting their involvement in higher-level rather than purely visual processing of numerical stimuli. Moreover, a subset of these math-selective pITG and aIPS neuronal populations respond nearly simultaneously during mathematical processing, despite a large anatomical distance between them. The math-selective neuronal populations within the pITG and aIPS exhibited selective functional coupling with each other during mathematical processing (and to a lesser degree during rest and nonmath conditions), relative to other active but less selective sites. Last, a trend in our data suggested a bidirectional relationship between the pITG and aIPS, with separate populations of neurons engaged in different directions of communication.

Numerical Processing in Discrete Neuronal Populations Within the Human Inferior Temporal Cortex. In line with our recent observation (37), we report the presence of a population of neurons in the pITG that has selective responses to the visual presentation of individual numerals, i.e., the NFA. This population is surrounded by a larger population of pITG neurons that is selectively engaged during the active manipulation of numerals. The latter population of neurons is part of a still larger region of the VTC that, compared with baseline, has nonselective responses to different classes of visual objects, as suggested by earlier pioneering ECoG work (33). That numeral-selective and math-selective populations of neurons are surrounded by populations with nonselective responses to these stimuli causes a significant methodological challenge for ECoG studies (such as our own) using sparse recordings and for neuroimaging studies that rely on group analysis and transfer of data from native to standardized anatomical space. These selective and nonselective populations may be spatially close but functionally unique, requiring fine-scale sampling in native anatomy.

Numerical Processing in Discrete Neuronal Populations Within the Human Lateral Parietal Cortex. Our findings in the LPC corroborate our previous work, showing a subregion in the aIPS region that is selectively activated when subjects solve mathematical equations in an experimental setting or when they deal with numerical entities in a naturalistic setting (20). One could argue that the activity we observe in the aIPS when subjects judge arithmetic equations as true or false (task 2) is not truly math specific but instead reflects more general externally directed attention or cognitive control functions and thus could be part of the dorsal attention network (69) or frontoparietal control network (70). However, the aIPS$_{math}$ sites did not exhibit any activity (even transiently) when subjects were attending to written statements during memory trials or were switching between task instructions at the beginning of each trial. Unlike the aIPS$_{math}$ region, the SPL and more posterior IPS activations had profiles matching those we would expect of regions in the dorsal attention or frontoparietal control network (i.e., transient responses at the beginning of both math and memory trials, as shown in Fig. S6*E*). The aIPS sites that were coupled with the pITG not only were significantly active during the math condition but also,

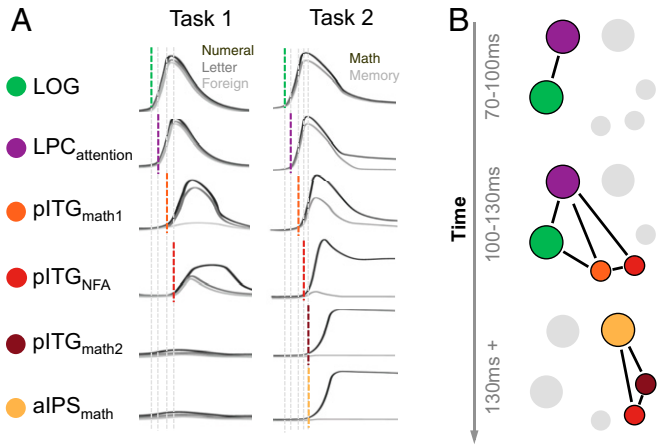

Fig. 8. (*A*) General activity profiles (in task 1 and task 2) observed within four VTC regions (three within the pITG) and two LPC regions that we propose are engaged in different aspects of numerical cognition (time courses shown are not real data). Vertical dotted lines indicate the timing of onset in these different brain regions. (*B*) Proposed sequence of coupling between the brain regions in *A*, with earlier VTC–LPC loops more engaged in visual processing/attention and later loops engaged in carrying out the arithmetic computation.

just as importantly, showed almost no activity during the memory condition (Fig. 3*D* and Figs. S5*A* and S6). Last, although many LPC sites outside the aIPS [e.g., in the SPL and posterior IPS (pIPS)] responded to individual numerals (and also to letters and false fonts; Fig. 3*B* and Fig. S3) in task 1, the $aIPS_{math}$ sites did not respond, even though subjects were actively attending to the numerals. Therefore, the activity of the $aIPS_{math}$ sites is unlikely to be related to general attention or even to selective attention to numerals. Instead, the $aIPS_{math}$ sites were active only when subjects were required to interpret and manipulate numerals actively in the context of judging arithmetic statements. The $aIPS_{math}$ region we identify here is anatomically similar to the parietal regions in which previous studies have observed numerosity tuning in humans (24, 71, 72) and in macaques (4, 73, 74). However, although we are confident about the selective functional engagement of $aIPS_{math}$ sites during numerical processing, we are cognizant that future work is needed to disentangle further the functional roles of the $aIPS_{math}$ sites and nearby sites within different domains of numerical cognition.

Task-Based and Intrinsic Coupling of Activity Across Neuronal Populations in the VTC and LPC. The pITG and aIPS were both highly engaged during arithmetic processing and were much less engaged during sentence reading/memory retrieval; thus their HFB activity was unsurprisingly correlated across all trials in task 2. However, variations in the neural responses within a single task condition (beyond the average response, i.e., noise) are thought to reflect fluctuations in endogenous activity or different "brain states" between trials (48–52). Therefore, our finding of selective noise correlations between the pITG and aIPS likely reflects the coupling of their endogenous activity; that coupling appears to be strongest during numerical processing but is still present during other nonnumeric task conditions (reading sentences/memory retrieval) and at rest. Importantly, the strength of coupling between the aIPS and different VTC sites within the math condition correlated with the VTC sites' selectivity rather than with the magnitude of their responses during the math condition (Fig. 6*E*). The same was true for correlations between the pITG and different LPC sites (Fig. S6*G*). Therefore it is unlikely that the selective correlation between the pITG and aIPS is simply an artifact of the simultaneous engagement of these regions. To support this claim further, the correlation between $aIPS_{math}$ and $pITG_{math}$ sites during memory trials was still stronger than the correlation between the $aIPS_{math}$ and other VTC sites (e.g., LOG/pFG) that exhibited larger HFB responses during memory trials (Fig. 2*B*).

Temporal Dynamics of Coupling Between the pITG and aIPS. The PAC and onset latency analyses provided additional clues about the nature of interaction between the math-selective hubs within the pITG and aIPS. Although on average the math-active sites within the pITG responded earlier than those within the aIPS, we observed nearly simultaneous engagement of the math-selective pITG and aIPS hubs in two of the three subjects in whom we were able to measure onset latencies in both the $pITG_{math}$ and $aIPS_{math}$. The sparse and slightly different electrode coverage across subjects likely explains the different times of onset between the pITG and aIPS across subjects. Specifically, the pITG populations selected in each patient may be engaged in different aspects of numerical computations (e.g., visual processing of symbols versus active arithmetic computations). Still, the nearly simultaneous engagement of subpopulations within the aIPS and pITG suggests that the pITG's role in numerical cognition is more complex than simply representing the symbolic numerical code.

Our PAC results, although preliminary, suggest a feedback loop between the pITG and aIPS with bottom-up coupling from pITG populations engaged in decoding individual numerals and top-down coupling to pITG populations more engaged in active arithmetic computations. The different coupling frequencies we observe across subjects raise intriguing questions that can be tested in future studies: Namely whether the frequency of slow oscillations that couple two distinct regions of the brain differs from one individual to another or is different across centimeters of cortex.

Last, the strong coupling from aIPS phase to pITG amplitude is interesting in light of a recent finding that the NFA region exhibits selectivity for numerical stimuli even in a congenitally blind person to whom numerical stimuli were presented auditorily (38). Our results support the biased connectivity hypothesis in regards to the development of the NFA (8): that the selectivity within the NFA may be driven by its intrinsic connectivity with the aIPS. However, such an interaction between the aIPS and pITG may be direct or indirect, possibly mediated by a third structure such as the thalamus, which plays a role in regulating information flow between cortical areas (75–77).

Conclusion

The current study revealed information about the patterns of electrophysiological activity within two regions of the human brain (VTC and LPC) that are predicted by the Triple Code model to be important for numerical processing and additionally about the nature of the coupling between them. Although addressing distinct cognitive aspects of numerical processing within each of these two regions was beyond the scope of this study, the high temporal resolution and anatomical precision of ECoG enabled us to gain insight into the complex functional heterogeneity within each region of the VTC and LPC and their distinct patterns of functional coupling. Within the VTC and LPC we were able to detect discrete neuronal populations (separated by as little as 5 mm) with significantly different profiles of activity across tasks (e.g., with some sites responding both to individual numerals and active arithmetic and other, neighboring sites responding only during active arithmetic processing but not during the presentation of individual numerals). This spatial specificity of task-related response profiles was mirrored in the correlations between the VTC and LPC in the spatially specific patterns of noise and spontaneous (i.e., rest) activity (Fig. 6 and Fig. S6). Moreover, preliminary results suggest different directions of communication (i.e., bottom-up versus top-down) between these different pITG and aIPS subpopulations (Fig. 7).

We believe that, taken together, the response profiles of different VTC and LPC subregions, their relative response times, and functional coupling patterns are suggestive of multiple feedback loops operating between different VTC and LPC subregions (Fig. 8). We propose that different loops are engaged during different stages of numerical processing and that in some cases neighboring sites (e.g., within the pITG) are engaged in different loops. Brain regions with early, transient, less-selective responses (e.g., the LOG, SPL, and pIPS) may form loops that are involved in visual processing of and attention to the visual stimuli, whereas other regions with later, sustained, and more math-selective responses (i.e., the $pITG_{math}$/NFA and $aIPS_{math}$) may form loops to carry out arithmetic computations (Fig. 8*B*). The NFA is possibly at the intersection of bottom-up visual processes and top-down processes from $aIPS_{math}$, given its response to individual symbols (and exhibiting a late selective response to numerals) and its sustained response during arithmetic processing. This very tentative, simplified model ignores regions such as the thalamus and frontal cortex that also are likely involved in numerical cognition. However, we hope that it can provide a general framework for future studies that can further disentangle the roles of these brain regions and their interactions in distinct aspects of numerical cognition.

Experimental Procedures

Subjects. Sixteen patients with epilepsy were implanted with intracranial electrodes as part of their presurgical evaluation at Stanford University Medical Center. Demographic information for each subject is included in Table S1, and each subject's electrode coverage is displayed in Fig. S1. Each patient was monitored in the hospital for ∼6–10 d following surgery. All subjects provided verbal and written consent before participating in any experiments. The experiments were approved by the Stanford Institutional Review Board.

Electrodes. Each subject was implanted with grids and/or strips of subdural platinum electrodes (AdTech Medical Instruments), whose locations were determined purely for clinical reasons (Fig. S1). Each electrode had an exposed diameter of 2.3 mm, with interelectrode spacing of 10 mm (5 mm for higher-density arrays).

Behavioral Paradigms. All tasks were conducted at the patient's bedside. Stimuli were presented visually on a laptop computer (Apple MacBook or MacBook Pro) with MATLAB psychtoolbox (see Fig. 1 for an illustration of all tasks).

Task 1. Subjects were presented visually with a series of symbols falling under one of three categories: (*i*) numerals, (*ii*) letters in the Roman alphabet, or (*iii*) letters in other alphabets. For each symbol, subjects had to press one button if they could read the symbol (i.e., numbers or letters in the Roman alphabet) and a different button if they could not read it (i.e., symbols in other alphabets). Subjects had up to 15 s to respond to each stimulus; trials were separated by a 500-ms ITI.

Task 2. Subjects were asked to make true/false judgments about a series of visually presented statements, requiring either memory (e.g., "I ate fruit yesterday") or arithmetic (e.g., "48 + 8 = 57") processing. Subjects had up to 15 s to respond to each statement by pressing one of two keypad buttons. These statements were interspersed with fixation periods (5 s or 10 s) during which subjects were asked to fixate at a center crosshair. A 200-ms ITI separated trials.

Task 3. Subjects were asked to make true/false judgments about arithmetic equations that were visually presented one numeral/symbol at a time (e.g., "7" "+" "5" "=" "12"). Each stimulus was presented for 500 ms with a 400-ms ITI. Subjects had up to 10 s to respond after the last number was presented. Trials were separated by a 2-s ITI.

Data Acquisition and Analysis. ECoG data were recorded from subdural electrodes via a multichannel recording system (Tucker David Technologies). Data were acquired with a bandpass filter of 0.5–300 Hz and a sampling rate of 1,525.88 Hz. The electrode outside the seizure zone with the most silent electrocorticographic activity was selected as an online reference during acquisition.

Preprocessing. Before data processing, electrodes identified as within the ictogenic zone or those corrupted by electrical noise were eliminated from subsequent analyses. Also excluded were electrodes whose overall power was five or more SDs above or below the mean power across channels and those whose power spectrum strayed from the normal 1/f power spectrum, based on visual inspection. All nonexcluded channels were notch filtered at 60 Hz and harmonics to remove electric interference and then were rereferenced to the mean of the filtered signals of the nonexcluded channels. The rereferenced signal at each electrode was then bandpass filtered into six different frequency bands, 1–3 Hz, 4–7 Hz, 8–12 Hz, 13–29 Hz, 30–55 Hz, and 70–180 Hz, using two-way, zero-lag, finite impulse response (FIR) filters. Instantaneous amplitude was computed by taking the modulus of the Hilbert-transformed signal. We subdivided the 70–180 Hz band (HFB) into bandpass windows with a width of 10 Hz (70–80 Hz, 80–90 Hz, and so forth) and normalized the amplitude of each 10-Hz band signal by its own mean, then averaged these normalized amplitude time series together, yielding a single-amplitude time course for the HFB band. This normalization procedure was applied to correct partially for the 1/frequency decay present in neurophysiological signals.

To evaluate the activity at each site on a finer spectral scale, we also generated spectrograms for each site displaying the time course of activity within smaller spectral bins. To generate spectrograms, we convolved the notch-filtered, common-average referenced signal with Gabor wavelet filters (span of five cycles) centered at 30 different frequencies (log-spaced between 1 and 256 Hz), yielding instantaneous amplitude estimates at each frequency and time point. The amplitude in each frequency bin then was normalized by the amplitude in that same frequency bin during the baseline (200-ms ITI) period, allowing us to see task-induced changes in spectral power relative to the baseline.

See *SI Experimental Procedures* for more details on analysis methods.

ACKNOWLEDGMENTS. We thank all the patients for volunteering their time to participate in this study; Pooya Ehsani, Jean-Rémi King, Dora Hermes, Zachary Greenberg, and other Laboratory of Behavioral and Cognitive Neuroscience team members for their help in the initial and early stages of this study; and Stanislas Dehaene for his important feedback throughout the project. This work was supported by research Grant R01NS078396 from the National Institute of Neurological Disorders and Stroke; Grant 1R01MH109954-01 from the National Institute of Mental Health (NIMH); Grant BCS1358907 from the National Science Foundation (NSF) (all to J.P.); Postdoctoral Fellowship 1F32HD087028-01 from the National Institute of Child Health and Human Development (to A.L.D.); Career Development Award K99MH103479 from the NIMH (to B.L.F.); NSF Graduate Research Fellowship DGE 1106400 (to V.R.); and a Marie Sklodowska-Curie Actions Fellowship, Project DecoMP_ECoG 654038 (to J.S.). The views presented in this work do not necessarily reflect those of the National Institutes of Health.

1. Lipton JS, Spelke ES (2003) Origins of number sense. Large-number discrimination in human infants. *Psychol Sci* 14(5):396–401.
2. Boysen ST, Berntson GG (1989) Numerical competence in a chimpanzee (*Pan troglodytes*). *J Comp Psychol* 103(1):23–31.
3. Brannon EM, Terrace HS (1998) Ordering of the numerosities 1 to 9 by monkeys. *Science* 282(5389):746–749.
4. Nieder A (2012) Supramodal numerosity selectivity of neurons in primate prefrontal and posterior parietal cortices. *Proc Natl Acad Sci USA* 109(29):11860–11865.
5. Brannon EM, Wusthoff CJ, Gallistel CR, Gibbon J (2001) Numerical subtraction in the pigeon: Evidence for a linear subjective number scale. *Psychol Sci* 12(3):238–243.
6. Ansari D (2008) Effects of development and enculturation on number representation in the brain. *Nat Rev Neurosci* 9(4):278–291.
7. Dehaene S (2011) *The Number Sense: How the Mind Creates Mathematics* (Oxford Univ Press, New York), 2nd Ed.
8. Hannagan T, Amedi A, Cohen L, Dehaene-Lambertz G, Dehaene S (2015) Origins of the specialization for letters and numbers in ventral occipitotemporal cortex. *Trends Cogn Sci* 19(7):374–382.
9. Cipolotti L, Butterworth B, Denes G (1991) A specific deficit for numbers in a case of dense acalculia. *Brain* 114(Pt 6):2619–2637.
10. Cohen L, Dehaene S (1995) [Reading numbers in pure alexia: Effects of the task and hemispheric specialization]. *Rev Neurol (Paris)* 151(8-9):480–485.
11. Dagenbach D, McCloskey M (1992) The organization of arithmetic facts in memory: Evidence from a brain-damaged patient. *Brain Cogn* 20(2):345–366.
12. Dehaene S, Cohen L (1991) Two mental calculation systems: A case study of severe acalculia with preserved approximation. *Neuropsychologia* 29(11):1045–1054.
13. McCloskey M, Caramazza A, Basili A (1985) Cognitive mechanisms in number processing and calculation: Evidence from dyscalculia. *Brain Cogn* 4(2):171–196.
14. Takayama Y, Sugishita M, Akiguchi I, Kimura J (1994) Isolated acalculia due to left parietal lesion. *Arch Neurol* 51(3):286–291.
15. Dehaene S (1992) Varieties of numerical abilities. *Cognition* 44(1-2):1–42.
16. Dehaene S, Cohen L (1995) Towards an anatomical and functional model of number processing. *Math Cogn* 1:83–120.
17. Arsalidou M, Taylor MJ (2011) Is 2+2=4? Meta-analyses of brain areas needed for numbers and calculations. *Neuroimage* 54(3):2382–2393.

18. Cantlon JF, Brannon EM, Carter EJ, Pelphrey KA (2006) Functional imaging of numerical processing in adults and 4-y-old children. *PLoS Biol* 4(5):e125.
19. Chochon F, Cohen L, van de Moortele PF, Dehaene S (1999) Differential contributions of the left and right inferior parietal lobules to number processing. *J Cogn Neurosci* 11(6):617–630.
20. Dastjerdi M, Ozker M, Foster BL, Rangarajan V, Parvizi J (2013) Numerical processing in the human parietal cortex during experimental and natural conditions. *Nat Commun* 4:2528.
21. Eger E, Sterzer P, Russ MO, Giraud AL, Kleinschmidt A (2003) A supramodal number representation in human intraparietal cortex. *Neuron* 37(4):719–725.
22. Nieder A, Dehaene S (2009) Representation of number in the brain. *Annu Rev Neurosci* 32:185–208.
23. Piazza M, Eger E (2016) Neural foundations and functional specificity of number representations. *Neuropsychologia* 83:257–273.
24. Piazza M, Izard V, Pinel P, Le Bihan D, Dehaene S (2004) Tuning curves for approximate numerosity in the human intraparietal sulcus. *Neuron* 44(3):547–555.
25. Walsh V (2003) A theory of magnitude: Common cortical metrics of time, space and quantity. *Trends Cogn Sci* 7(11):483–488.
26. Butterworth B, Varma S, Laurillard D (2011) Dyscalculia: From brain to education. *Science* 332(6033):1049–1053.
27. Moeller K, Willmes K, Klein E (2015) A review on functional and structural brain connectivity in numerical cognition. *Front Hum Neurosci* 9:227.
28. Matejko AA, Ansari D (2015) Drawing connections between white matter and numerical and mathematical cognition: A literature review. *Neurosci Biobehav Rev* 48: 35–52.
29. Jolles D, et al. (2016) Parietal hyper-connectivity, aberrant brain organization, and circuit-based biomarkers in children with mathematical disabilities. *Dev Sci* 19(4): 613–631.
30. Iuculano T, Cohen Kadosh R (2014) Preliminary evidence for performance enhancement following parietal lobe stimulation in developmental dyscalculia. *Front Hum Neurosci* 8:38.
31. Salillas E, Semenza C, Basso D, Vecchi T, Siegal M (2012) Single pulse TMS induced disruption to right and left parietal cortex on addition and multiplication. *Neuroimage* 59(4):3159–3165.
32. Andres M, Pelgrims B, Michaux N, Olivier E, Pesenti M (2011) Role of distinct parietal areas in arithmetic: An fMRI-guided TMS study. *Neuroimage* 54(4):3048–3056.
33. Allison T, Puce A, Spencer DD, McCarthy G (1999) Electrophysiological studies of human face perception. I: Potentials generated in occipitotemporal cortex by face and non-face stimuli. *Cereb Cortex* 9(5):415–430.
34. Park J, Hebrank A, Polk TA, Park DC (2012) Neural dissociation of number from letter recognition and its relationship to parietal numerical processing. *J Cogn Neurosci* 24(1):39–50.
35. Pinel P, Dehaene S, Rivière D, LeBihan D (2001) Modulation of parietal activation by semantic distance in a number comparison task. *Neuroimage* 14(5):1013–1026.
36. Price GR, Ansari D (2011) Symbol processing in the left angular gyrus: Evidence from passive perception of digits. *Neuroimage* 57(3):1205–1211.
37. Shum J, et al. (2013) A brain area for visual numerals. *J Neurosci* 33(16):6709–6715.
38. Abboud S, Maidenbaum S, Dehaene S, Amedi A (2015) A number-form area in the blind. *Nat Commun* 6:6026.
39. Grotheer M, Herrmann KH, Kovács G (2016) Neuroimaging evidence of a bilateral representation for visually presented numbers. *J Neurosci* 36(1):88–97.
40. Hermes D, et al. (October 26, 2015) Electrophysiological responses in the ventral temporal cortex during reading of numerals and calculation. *Cereb Cortex*, 10.1093/cercor/bhv250.
41. Schrouff J, Mourão-Miranda J, Phillips C, Parvizi J (2016) Decoding intracranial EEG data with multiple kernel learning method. *J Neurosci Methods* 261:19–28.
42. Manning JR, Jacobs J, Fried I, Kahana MJ (2009) Broadband shifts in local field potential power spectra are correlated with single-neuron spiking in humans. *J Neurosci* 29(43):13613–13620.
43. Ray S, Maunsell JH (2011) Different origins of gamma rhythm and high-gamma activity in macaque visual cortex. *PLoS Biol* 9(4):e1000610.
44. Logothetis NK, Pauls J, Augath M, Trinath T, Oeltermann A (2001) Neurophysiological investigation of the basis of the fMRI signal. *Nature* 412(6843):150–157.
45. Flinker A, Chang EF, Barbaro NM, Berger MS, Knight RT (2011) Sub-centimeter language organization in the human temporal lobe. *Brain Lang* 117(3):103–109.
46. Parvizi J, et al. (2012) Electrical stimulation of human fusiform face-selective regions distorts face perception. *J Neurosci* 32(43):14915–14920.
47. Foster BL, Rangarajan V, Shirer WR, Parvizi J (2015) Intrinsic and task-dependent coupling of neuronal population activity in human parietal cortex. *Neuron* 86(2): 578–590.
48. Lewis CM, Bosman CA, Womelsdorf T, Fries P (2016) Stimulus-induced visual cortical networks are recapitulated by spontaneous local and interareal synchronization. *Proc Natl Acad Sci USA* 113(5):E606–E615.
49. Luczak A, Barthó P, Harris KD (2009) Spontaneous events outline the realm of possible sensory responses in neocortical populations. *Neuron* 62(3):413–425.
50. Kenet T, Bibitchkov D, Tsodyks M, Grinvald A, Arieli A (2003) Spontaneously emerging cortical representations of visual attributes. *Nature* 425(6961):954–956.
51. Arieli A, Sterkin A, Grinvald A, Aertsen A (1996) Dynamics of ongoing activity: Explanation of the large variability in evoked cortical responses. *Science* 273(5283): 1868–1871.
52. Tsodyks M, Kenet T, Grinvald A, Arieli A (1999) Linking spontaneous activity of single cortical neurons and the underlying functional architecture. *Science* 286(5446): 1943–1946.
53. Keller CJ, et al. (2013) Neurophysiological investigation of spontaneous correlated and anticorrelated fluctuations of the BOLD signal. *J Neurosci* 33(15):6333–6342.
54. Leopold DA, Logothetis NK (2003) Spatial patterns of spontaneous local field activity in the monkey visual cortex. *Rev Neurosci* 14(1-2):195–205.
55. Nir Y, et al. (2008) Interhemispheric correlations of slow spontaneous neuronal fluctuations revealed in human sensory cortex. *Nat Neurosci* 11(9):1100–1108.
56. He BJ, Snyder AZ, Zempel JM, Smyth MD, Raichle ME (2008) Electrophysiological correlates of the brain's intrinsic large-scale functional architecture. *Proc Natl Acad Sci USA* 105(41):16039–16044.
57. Hipp JF, Hawellek DJ, Corbetta M, Siegel M, Engel AK (2012) Large-scale cortical correlation structure of spontaneous oscillatory activity. *Nat Neurosci* 15(6):884–890.
58. Varela F, Lachaux JP, Rodriguez E, Martinerie J (2001) The brainweb: Phase synchronization and large-scale integration. *Nat Rev Neurosci* 2(4):229–239.
59. Fries P (2005) A mechanism for cognitive dynamics: Neuronal communication through neuronal coherence. *Trends Cogn Sci* 9(10):474–480.
60. Buzsaki G (2011) *Rhythms of the Brain* (Oxford Univ Press, New York) 1st Ed.
61. Canolty RT, et al. (2006) High gamma power is phase-locked to theta oscillations in human neocortex. *Science* 313(5793):1626–1628.
62. Miller KJ, et al. (2010) Dynamic modulation of local population activity by rhythm phase in human occipital cortex during a visual search task. *Front Hum Neurosci* 4:197.
63. Voytek B, et al. (2015) Oscillatory dynamics coordinating human frontal networks in support of goal maintenance. *Nat Neurosci* 18(9):1318–1324.
64. Watrous AJ, Deuker L, Fell J, Axmacher N (2015) Phase-amplitude coupling supports phase coding in human ECoG. *eLife* 4:07886, erratum in *eLife* (2015) 4:12810.
65. Foster BL, Parvizi J (2012) Resting oscillations and cross-frequency coupling in the human posteromedial cortex. *Neuroimage* 60(1):384–391.
66. Voytek B, et al. (2010) Shifts in gamma phase-amplitude coupling frequency from theta to alpha over posterior cortex during visual tasks. *Front Hum Neurosci* 4:191.
67. van der Meij R, Kahana M, Maris E (2012) Phase-amplitude coupling in human electrocorticography is spatially distributed and phase diverse. *J Neurosci* 32(1):111–123.
68. Maris E, van Vugt M, Kahana M (2011) Spatially distributed patterns of oscillatory coupling between high-frequency amplitudes and low-frequency phases in human iEEG. *Neuroimage* 54(2):836–850.
69. Corbetta M, Shulman GL (2002) Control of goal-directed and stimulus-driven attention in the brain. *Nat Rev Neurosci* 3(3):201–215.
70. Dosenbach NU, et al. (2007) Distinct brain networks for adaptive and stable task control in humans. *Proc Natl Acad Sci USA* 104(26):11073–11078.
71. Harvey BM, Klein BP, Petridou N, Dumoulin SO (2013) Topographic representation of numerosity in the human parietal cortex. *Science* 341(6150):1123–1126.
72. Eger E, Pinel P, Dehaene S, Kleinschmidt A (2015) Spatially invariant coding of numerical information in functionally defined subregions of human parietal cortex. *Cereb Cortex* 25(5):1319–1329.
73. Nieder A, Miller EK (2004) A parieto-frontal network for visual numerical information in the monkey. *Proc Natl Acad Sci USA* 101(19):7457–7462.
74. Roitman JD, Brannon EM, Platt ML (2007) Monotonic coding of numerosity in macaque lateral intraparietal area. *PLoS Biol* 5(8):e208.
75. Saalmann YB, Kastner S (2011) Cognitive and perceptual functions of the visual thalamus. *Neuron* 71(2):209–223.
76. Zikopoulos B, Barbas H (2007) Circuits formultisensory integration and attentional modulation through the prefrontal cortex and the thalamic reticular nucleus in primates. *Rev Neurosci* 18(6):417–438.
77. Steriade M, McCormick DA, Sejnowski TJ (1993) Thalamocortical oscillations in the sleeping and aroused brain. *Science* 262(5134):679–685.
78. Hermes D, Miller KJ, Noordmans HJ, Vansteensel MJ, Ramsey NF (2010) Automated electrocorticographic electrode localization on individually rendered brain surfaces. *J Neurosci Methods* 185(2):293–298.
79. Schrouff J, et al. (2013) PRoNTo: Pattern recognition for neuroimaging toolbox. *Neuroinformatics* 11(3):319–337.